Origin of the Magnetic Exciton in the van der Waals Antiferromagnet $NiPS_3$

T. Klaproth,[1] S. Aswartham,[1] Y. Shemerliuk,[1] S. Selter,[1] O. Janson,[1] J. van den Brink,[1] B. Büchner,[1,2] M. Knupfer,[1] S. Pazek,[1] D. Mikhailova,[1] A. Efimenko,[3,4] R. Hayn,[5] A. Savoyant,[5] V. Gubanov,[5] and A. Koitzsch[1]

[1]*Leibniz Institute for Solid State and Materials Research Dresden, Helmholtzstrasse 20, 01069 Dresden, Germany*
[2]*Institute of Solid State and Material Physics, Technische Universität Dresden, 01062 Dresden, Germany*
[3]*Helmholtz-Zentrum Berlin für Materialien und Energie, Interface Design, Albert Einstein Str. 15, 12489 Berlin, Germany*
[4]*Helmholtz Zentrum Berlin für Materialien und Energie, Energy Materials In-situ Laboratory Berlin (EMIL), Albert Einstein Str. 15, 12489 Berlin, Germany*
[5]*Aix-Marseille Université, Centre National de la Recherche Scientifique, IM2NP-UMR 7334, 13397 Marseille Cedex 20, France*

(Received 16 May 2023; revised 29 September 2023; accepted 3 October 2023; published 21 December 2023)

An ultrasharp photoluminescence line intimately related to antiferromagnetic order has been found in $NiPS_3$, a correlated van der Waals material, opening prospects for magneto-optical coupling schemes and spintronic applications. Here we unambiguously clarify the singlet origin of this excitation, confirming its roots in the spin structure. Based on a comprehensive investigation of the electronic structure using angle-resolved photoemission and q-dependent electron energy loss spectroscopy as experimental tools we develop, in a first step, an adequate theoretical understanding using density functional theory (DFT). In a second step the DFT is used as input for a dedicated multiplet theory by which we achieve excellent agreement with available multiplet spectroscopy. Our Letter connects the understanding of the electronic structure and of optical processes in $NiPS_3$ and related materials as a prerequisite for further progress of the field.

DOI: 10.1103/PhysRevLett.131.256504

Transition metal trichalcogenides of the type $TMPS_3$ are one of the material classes that are now forcefully shifting to the scientific focus due to the rise of magnetic 2D materials. They possess a layered crystal structure and are often antiferromagnets. $NiPS_3$ in particular features *zigzag* type antiferromagnetism almost down to the monolayer [1]. Miniaturization of electronic devices is one of the driving forces for the immense interest in 2D materials. Naturally, magnetic materials may serve as memory media and so far mostly ferromagnets are used. However, antiferromagnets hold some prospects, such as high-speed and low-power operation and long time stability, but it is notoriously difficult to detect and control the magnetic state by electrical or optical means. At this point $NiPS_3$ is exceptional and shows much potential.

In an impressive row of papers an intimate entanglement of electronic, magnetic, and optical properties has been reported recently [2–8]. In particular, the optical excitation across the gap depends on the appearance of magnetic order, which is unusual and connected to the correlated nature of the electronic structure of $NiPS_3$ [2]. But the most surprising optical property of $NiPS_3$ is undoubtedly the appearance of ultrasharp, highly polarized, excitations below T_N inside the electronic energy gap, which have been assigned to magnetic excitons and which are easily accessible by standard optical methods like photoluminescence and absorption [3–6,9].

In order to make further progress, their exact nature needs to be settled. Kang *et al.* associated the excitons with a Zhang-Rice singlet-triplet transition [3] but further confirmation is necessary. In particular, exact knowledge of the electronic structure is indispensable. First optical and photoemission experiments on $NiPS_3$ date back to the late 1970s and early 1980s [10–12], followed by investigations using resonant photoemission [13–17], x-ray absorption spectroscopy [18,19], x-ray emission spectroscopy [20], and electron energy loss spectroscopy (EELS) [21]. $NiPS_3$ has been classified as a charge transfer insulator with significant coupling of spin and charge degrees of freedom [2,16,17]. Recently, the thickness dependence down to three atomic layers has been studied by resonant inelastic x-ray scattering (RIXS) and a reduction of the charge transfer energy and the relevant hopping parameters has been found [22].

Here we provide a comprehensive investigation of the electronic structure of $NiPS_3$ including angle-resolved photoemission spectroscopy (ARPES), EELS, DFT, and multiplet calculations. We elucidate the intertwined nature of electronic and magnetic properties and disclose the singlet origin of the magnetic exciton.

$NiPS_3$ single crystals were grown in a two-step process involving solid state synthesis of powders and a chemical vapor transport reaction. The photoemission data were measured using a NanoESCA system (Scienta Omicron) equipped with a HIS-13 helium lamp (He I: 21.2 eV, He II:

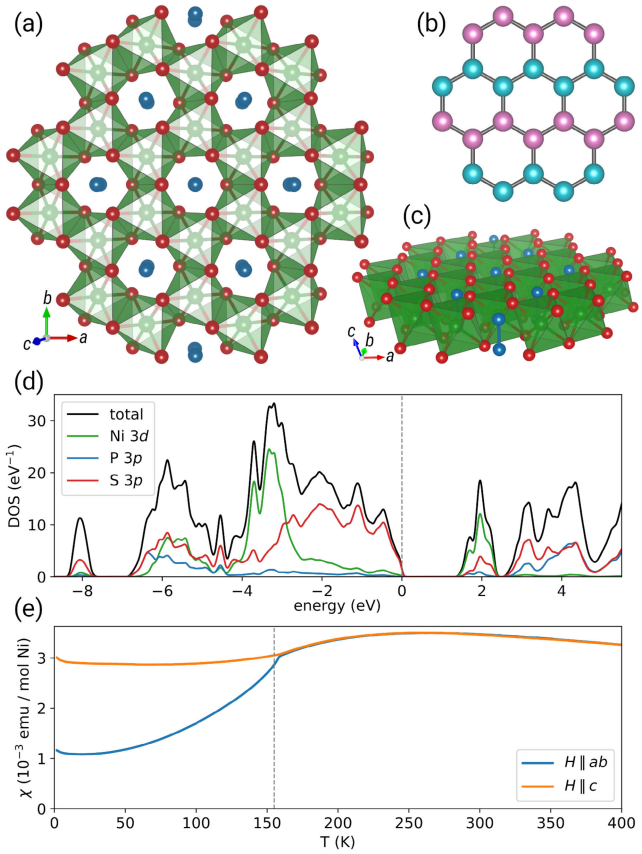

FIG. 1. (a) Projected in-plane crystal structure of $NiPS_3$. (sulphur, red; phosphor, blue) (b) Illustration of the zigzag antiferromagnetic order. Shown are the Ni ions only. (c) Side view of the crystal plane. (d) Density of states derived from DFT + U. (e) Susceptibility measurements of $NiPS_3$ indicating the antiferromagnetic phase transition at $T_N = 155$ K.

40.8 eV) at $T = 300$ K. The EELS measurements were carried out using a purpose built transmission electron energy-loss spectrometer with a primary electron energy of 172 keV [23]. DFT calculations were performed using the full-potential local-orbital code FPLO version 18 [24]. For the exchange and correlation potential, we used the generalized gradient approximation (GGA) by Perdew, Burke, and Ernzerhof [25]. Based on the DFT results, multiplet calculations have been conducted using the ELISA program [26]. Further details on crystal growth, sample preparation, spectroscopic measurements, DFT, and multiplet calculations are provided in the Supplemental Material [27].

$NiPS_3$ has a layered crystal structure with a honeycomb lattice of the Ni^{2+} ions (d^8 configuration), which are each surrounded by six sulfur atoms forming trigonally elongated octahedra [see Fig. 1(a)]. The d-manifold splits into three fully occupied t_{2g} and two half filled e_g levels. This results in local magnetic moments which order antiferromagnetically below $T_N = 155$ K [see Fig. 1(e)]. Figure 1(b) depicts the specific type of the antiferromagnetic pattern, a *zigzag* arrangement. Figure 1(c) presents a side view of the plane. The voids of the edge sharing octahedra network are filled by P_2 dimers. Coming to the electronic structure, Fig. 1(d) presents a calculation of the partial density of states (PDOS) of Ni $3d$, S $3p$, and P $3p$ by DFT + U. U has been set to $U = 4$ eV following earlier studies [2,33]. Our DFT + U calculations correctly reproduce the magnetic ground state: The zigzag AFM configuration yields the lowest total energy but other magnetic configurations are within thermal reach. To account for these contributions, we computed a Boltzmann-weighted sum of DOS at $T = 300$ K and plotted it in Fig. 1(d). The calculation reproduces the insulating ground state of $NiPS_3$ with a gap of $E_g \approx 1$ eV. The highest occupied states are dominated by S $3p$ whereas the Ni $3d$ levels are shifted back by the impact of U. Qualitatively, one finds broad S $3p$ bands intercepted by narrow Ni $3d$ bands. The lowest unoccupied states, on the other hand, are mainly of Ni $3d$ character.

Figure 2(a) shows valence bands measured with varying photon energies ($h\nu = 21.2$, 40.8 eV). According to cross section tables for $h\nu = 40.8$ eV, Ni $3d$ dominates whereas for $h\nu = 21.2$ eV S $3p$ weights in three times more than Ni $3d$ [34]. Spectral shape depends strongly on photon energy but clear correspondence of features exists, e.g., the three prominent peaks A, B, C between 0 and −2 eV of the $h\nu = 40.8$ eV spectrum appear as shoulders for $h\nu = 21.2$ eV, consistent with earlier less resolved results [15]. The high energy region of the $h\nu = 21.2$ eV spectrum compares well to the PDOS of S $3p$ and P $3p$ orbitals obtained by DFT + U. We have applied a modest renormalization factor of $r \approx 1.2$ to the energy axis, correcting a slight overestimation of the DFT bandwidth, and a shift towards larger energy. At low energy, deviations occur due to the contribution of Ni $3d$. The Ni $3d$ contribution is significantly shifted and renormalized compared to the DOS calculation in Fig. 1(c), reflecting their localized and correlated character. In fact, we find excellent agreement of the h$\nu = 40.8$ eV spectrum to a NiO_6 cluster calculation in O_h symmetry [35].

We observe quasiflat Ni $3d$ bands by ARPES [Fig. 2(d)] confirming their localized character. In contrast, the angle-resolved spectra of the S $3p$ states reveal strongly dispersing bands [Fig. 2(b)]. The experimental data are compared to DFT + U in Figs. 2(c) and 2(e) based on S $3p$ and Ni $3d$ orbital weight, respectively. Bandwidth renormalization factors and energy shifts have been applied ($r^{\mathrm{S}\,3p} \approx 1.2, r^{\mathrm{Ni}\,3d} \approx 2.8$). For $h\nu = 21.2$ eV especially the "V" shaped structures centered at M between −3 and −5 eV coincide with experiment. The insets of Fig. 2(e) present constant energy maps along with the surface Brillouin zone calculated from structural data [36]. The left inset provides a map at $E = -2.8$ eV ($h\nu = 21.2$ eV) illustrating the underlying sixfold symmetry. The right inset cuts the maximum of the Ni $3d$ band emission at $E = -1$ eV for $h\nu = 40.8$ eV [see Fig. 2(d)]. The intensity is rather

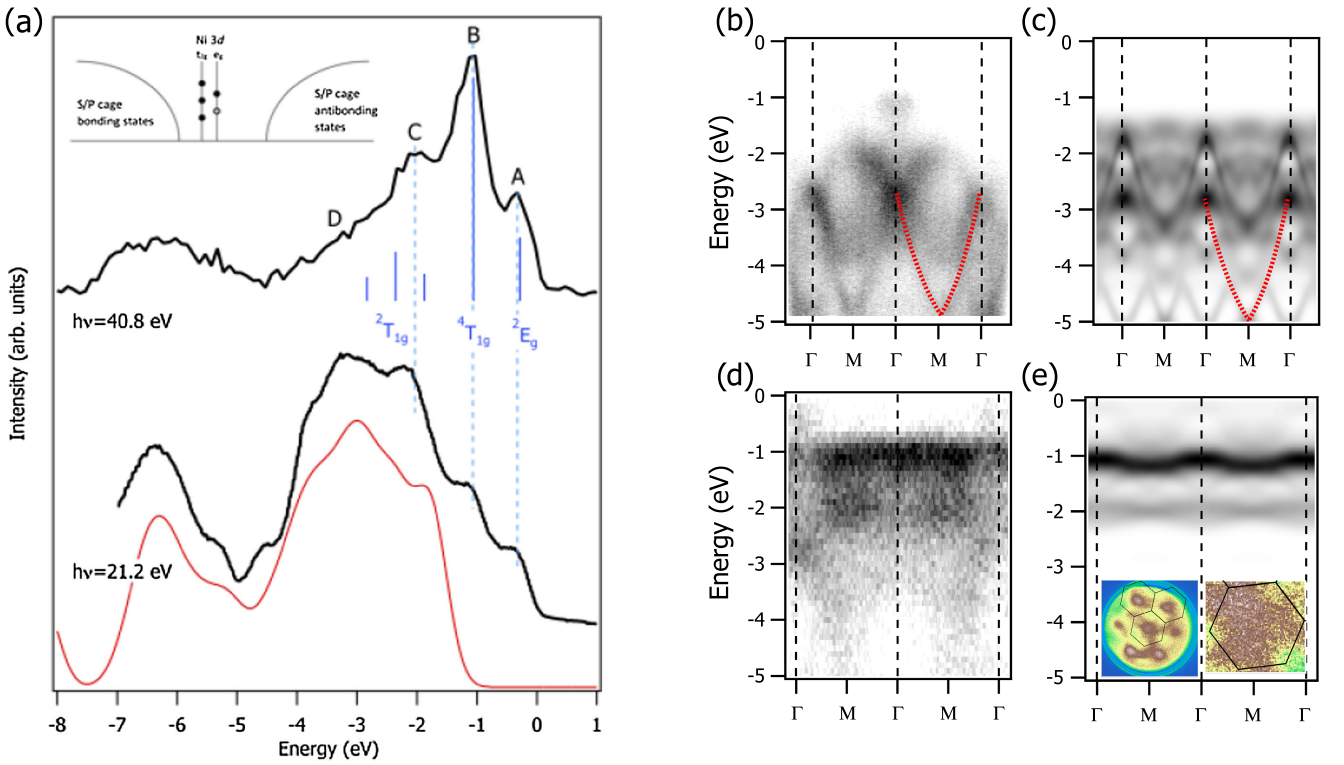

FIG. 2. (a) Angle-integrated photoemission spectroscopy of $NiPS_3$ at different photon energies. An integral background has been subtracted. Energy zero refers to top of the valence band. Inset: Simple view on the electronic structure of transition metal trichalcogenides. Blue bars represent the results of a cluster calculation reproduced from Ref. [35]. Red spectrum at the bottom corresponds to the S $3p$ + P $3p$ DOS. (b),(d) Experimental EDM along ΓM taken with $h\nu = 21.2$ (b) and $h\nu = 40.8$ eV (d) radiation. (c),(e) DFT derived energy distribution map (EDM) along ΓM of the S $3p$ (c) and Ni $3d$ (e) band weight. Inset: Constant energy maps at $E = -2.8$ eV ($h\nu = 21.2$ eV) and $E = -1$ eV ($h\nu = 40.8$ eV with surface Brillouin zone).

evenly distributed over large parts of the Brillouin zone confirming the absence of substantial dispersion of the d bands.

Based on early reflectance measurements Khumalo *et al.* proposed a model of the electronic structure of $NiPS_3$ and other transition metal trichalcogenides where the transition metal d states form sharply localized levels within broad bands formed by the P_2S_6 lattice, which remains constant with respect to the specific transition metal ion [37]. This scheme is depicted as an inset in Fig. 2(a). Our photoemission results corroborate this model inasmuch as we observe broad dispersing sulfur bands and localized quasi-flat Ni bands at the low energy side cutting the sulfur bands.

So far, we considered the occupied density of states. In order to investigate the unoccupied density of states we applied x-ray absorption spectroscopy (XAS) and core level EELS. Figures 3(a) and 3(b) present XAS data from polycrystalline material at the phosphorus and sulfur K edge. The near edge fine structure is determined by the unoccupied P and S $3p$ PDOS. The comparison works out well if bandwidth renormalization is taken into account ($r_{PK}^{\mathrm{XAS}} = 1.3, r_{SK}^{\mathrm{XAS}} = 2.4$). However, the Ni $3d$ PDOS cannot be determined in the same way since multiplet effects become again important. Figure 3(c) shows the Ni $L_{3,2}$ edge measured by EELS, which is in principle equivalent to XAS. The spectrum in Fig. 3(c) resembles previous XAS measurements [2] although the polarization geometry differs. From the latter we conclude that the trigonal distortion is relatively small. The experimental data are compared to a multiplet calculation explained in detail below. The main features coincide such as the narrow main L_3 peak at $E = 853.5$ eV followed by a satellite structure which is shifted somewhat in energy.

Figure 4 shows the low energy EELS intensity at low and high temperature in the optical limit, i.e., with small momentum transfer. We find a gapped spectrum with low intensity at low energies and an onset around $E = 1.6$ eV rising to a peak at $E = 2.4$ eV (peak A) and multiple peak structures at higher energies sitting on a smoothly increasing background. The lowest energy feature is a very weak peak at $E \approx 1$ eV, which has been previously associated with dipole forbidden onsite $d - d$ excitations [11,38]. Closer inspection of the rising flank of the main peak A reveals another small peak (see Supplemental Material [27] for further discussion).

According to the density of states and according to our discussion of the photoemission and x-ray absorption

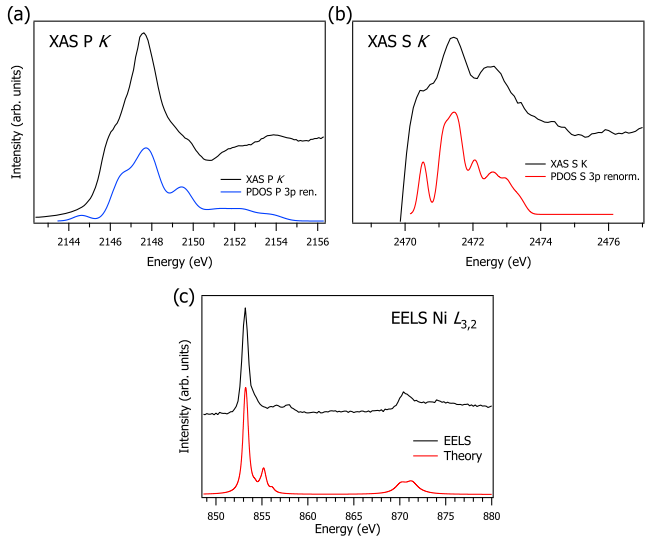

FIG. 3. (a) P K absorption edge compared to P $3p$ partial DOS. (b) S K absorption edge compared to S $3p$ partial DOS with bandwidth renormalization. A vertical offset has been applied to the PDOS for better comparison to the edge fine structure. (c) Ni $L_{3,2}$ EEL edge compared to multiplet theory.

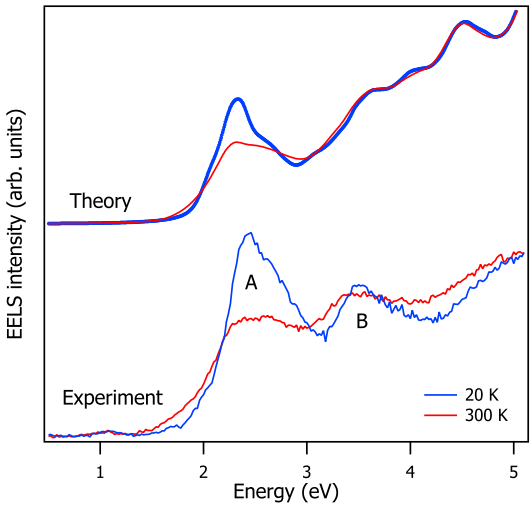

FIG. 4. Lower: EEL spectra at $T = 20$ and $T = 300$ K with small momentum transfer ($\boldsymbol{q} = 0.07$ Å). Upper: Calculated loss function. A renormalization factor has been applied to the energy axis [39].

spectra, the first excited state (peak A) should involve a charge transfer between S $3p$ and Ni $3d$. The large temperature dependence of peak A is an unusual effect and suggests a coupling of the electronic states to the underlying magnetic order below T_N similar to other correlated materials [40,41]. This observation confirms earlier measurements of the optical conductivity [2]. Figure 4 contains a calculation of the loss function and its temperature dependence based on DFT + U discussed above. The $T = 300$ K spectrum in Fig. 4 represents a Boltzmann weighted sum of all possible configurations (see Supplemental Material [27]). The calculated result agrees well with the experimental data. The higher lying magnetic configurations inevitably enforce a different charge distribution that finally alters the dielectric response. Note, that we have again applied a renormalization of the energy axis by $r^{\mathrm{EELS}} = 1.44$ taking into account the two-particle origin of L and an energy shift.

We have also measured the $\boldsymbol{q}$ dependence of the EEL spectra (see Supplemental Material [27]). The overall dispersion of the low energy peaks A and B is small consistent with the small dispersion seen in ARPES. However, a slight shift of peak A to higher energies for increasing $\boldsymbol{q}$ is present, implying a direct gap or an indirect gap with small momentum mismatch.

The temperature dependence of the gap excitation observed in EELS is a consequence of the coupled magnetic and electronic sector. Another purported consequence is the appearance of a sharp magnetic exciton at $E \approx 1.5$ eV seen in optical spectroscopies and RIXS [3–7]. It has been interpreted as a triplet-singlet transition, i.e., a local multipletlike excitation within a Ni-ligand complex.

In order to connect our DFT description of the low energy electronic structure with the local multiplets we use *ab initio* based multiplet theory [42], which is based on Wannerization of the nonmagnetic GGA band structure using maximally projected Wannier orbitals [43]. Here we concentrate on the Ni^{2+} $3d$ orbitals that hybridize with the neighboring S $3p$ ligand orbitals in trigonal symmetry (point group D_{3d}) giving rise to molecular like orbitals for which we build a local model with all Coulomb and spin-orbit (SO) parameters. The local many body problem is solved by exact diagonalization using the ELISA program. The ligand-field energies for cubic octahedral symmetry with small trigonal distortion are (in eV): $\Delta = -0.912$, $\nu = -0.085$, $\nu' = -0.021$. A first orientation for the Coulomb and SO parameters of the molecularlike orbitals is given by the free ion values $F(2) = 9.8$, $F(4) = 6.1$, $\xi = 0.080$. However, by reducing the Coulomb parameters within the $3d$ shell to 77% of their free ion value $[F(2) = 7.55, F(4) = 4.70]$ we can improve the comparison with the experimental RIXS spectrum and we will use these reduced Coulomb parameters in our present analysis.

Figure 5 presents the comparison of RIXS data reproduced from Ref. [3] to the calculation described above, where we applied an appropriate Gaussian broadening to the multiplet states leaving the spectral weight of the peaks constant. Satisfactory agreement is found for the low energy region $E \leq 1.5$ eV. But also at higher energies all the experimental peaks have a theoretical counterpart matching in intensity and fine structure albeit shifted in energy. Note that we have carried out our multiplet calculations with no adjustable parameters, as it is usually done, solely based on DFT. It is not surprising that the

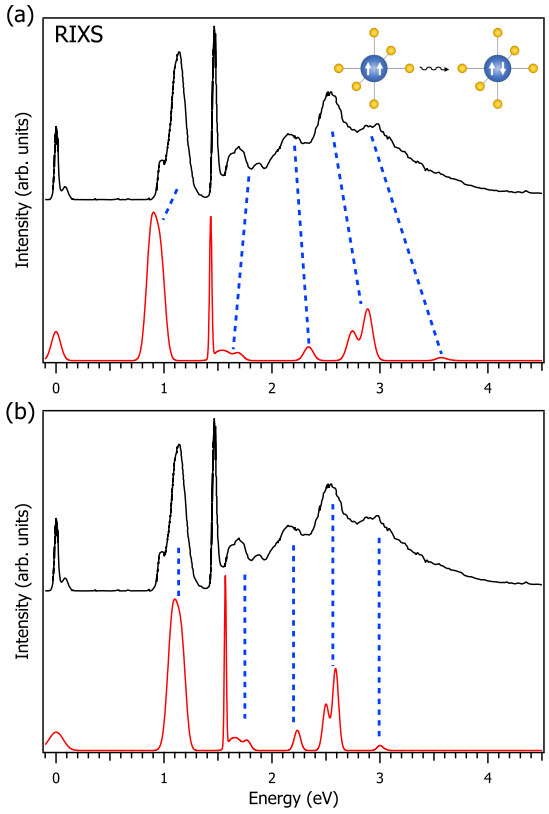

FIG. 5. (a) RIXS data reproduced from Ref. [3] in comparison to multiplet calculations after Wannerization of the DFT results. *Inset:* Schematic view on the triplet-singlet excitation. (b) Same as (a) but with exponential rescaling of the energy axis.

Wannerization over- or underestimates somewhat the crystal field parameters which shift the multiplet states in energy. Figure 5(b) presents the same dataset but now the energy axis has been rescaled by an exponential factor. Again the spectral weight of the peaks is preserved. It becomes clear that our theory gives an excellent description of the experimental multiplet states on a semiquantitative level. In particular, the sharp peak at 1.5 eV stems unambiguously from a singlet excitation if spin-orbit coupling is not taken into account. It gets mixed with triplets in the complete list of states (see Supplemental Material [27]) once spin-orbit coupling is finite. Since the ground state is of triplet character, the spin state is changed. Concerning the orbital character of the magnetic exciton, it has been shown that it resonates at the energy corresponding to d^9L in RIXS [3] and has predominant p-d character from theoretical analysis within an extended Hubbard model [8].

Excitons have been discussed before occasionally in the context of strongly correlated magnetic materials, but the underlying microscopic mechanisms are not always the same. A Zhang-Rice singlet exciton has been identified by Monney *et al.* in low dimensional cuprates [44]. Similarly to $NiPS_3$, this exciton is embedded in crystal field excitations and shows a strong temperature dependence. But it lacks the sharpness of the $NiPS_3$ exciton and it could be shown that it roots in a process involving neighboring plaquettes. A spin-orbit exciton, i.e., the excitation between different J states, dressed by magnons was identified in Sr_2IrO_4 [45]. Similar excitons have been discussed for α-$RuCl_3$ [46–48].

The observed exciton in $NiPS_3$ is extraordinarily sharp and it possesses a strong temperature dependence indicating an intimate relationship to magnetic order. However, the microscopic character of this relationship is not obvious. The temperature dependence of the exciton is in line with the temperature dependence of the charge-transfer gap transition A of the low energy EELS response (Fig. 4) reflecting the predominant d^9L character of the exciton observed by RIXS [3]. To simulate this temperature dependence, we computed the loss functions and the total energies of different magnetic configurations with zero net magnetization. Thermal-averaged loss functions at 20 and 300 K (Fig. 4) generally agree with the experiment. Microscopically, Dirnberger *et al.* showed that the transition strength of the S $3p \rightarrow$ Ni $3d$ charge transfer is linked to magnetic order by employing an extended Hubbard model [8]. The discussion of the magnetic exciton as an effective triplet-singlet on-site excitation leaves open the question of how this excitation becomes optically active, i.e., how the optical selection rules are satisfied. We have shown that the final state is influenced by significant spin-orbit coupling, hence the spin conservation rule might be sufficiently relaxed. In addition, it has been suggested before that the excitation process also induces a redistribution of charge between Ni $3d$ and S $3p$ orbitals generating an effective dipole moment [3,8].

Our results provide the understanding of how exactly the ultrasharp photoluminescence active mode at $E \approx 1.5$ eV roots in the electronic structure, which opens perspectives to enhance control over the underlying antiferromagnetic state. On a broader scope, trichalcogenides, and $NiPS_3$, in particular, have been and are interesting materials for a variety of other reasons; e.g., as host structures for intercalation of Li and other alkali metals in metal-ion batteries or the occurrence of large optical anisotropies [49], all of which require detailed knowledge of the electronic structure.

In conclusion, we have thoroughly studied the electronic structure of $NiPS_3$ by photoemission spectroscopy and EELS on the one hand and theoretical tools (DFT, multiplet calculations) on the other hand. We achieve comprehensive understanding of the one-particle and two-particle response. Based on this knowledge we unambiguously identify the exciton mode at $E \approx 1.5$ eV as an excitation of dominant triplet-singlet character, thereby clarifying its origin in the complex spin structure of $NiPS_3$.

Note added.— Recently, a related work by Yan *et al.* [50] appeared, reporting similar ARPES and DFT results.

This work was supported by the DFG (SFB 1143, Project No. 247310070). O. J. was supported by the Leibniz Association through the Leibniz Competition. S. A. acknowledges support by DFG (AS 523/4-1). A. K. acknowledges support by DFG grant KO 3831/9-1. A. K. and T. K. thank Roland Hübel, Frauke Thunig, and Marco Naumann for technical assistance. We used the FPLO computer code for the band structure calculations and we thank U. Nitzsche for technical assistance.

[1] K. Kim, S. Y. Lim, J.-U. Lee, S. Lee, T. Y. Kim, K. Park, G. S. Jeon, C.-H. Park, J.-G. Park, and H. Cheong, Suppression of magnetic ordering in XXZ-type antiferromagnetic monolayer $NiPS_3$, Nat. Commun. **10**, 345 (2019).

[2] S. Y. Kim, T. Y. Kim, L. J. Sandilands, S. Sinn, M.-C. Lee, J. Son, S. Lee, K.-Y. Choi, W. Kim, B.-G. Park, C. Jeon, H.-D. Kim, C.-H. Park, J.-G. Park, S. J. Moon, and T. W. Noh, Charge-spin correlation in van der Waals antiferromagnet $NiPS_3$, Phys. Rev. Lett. **120**, 136402 (2018).

[3] S. Kang, K. Kim, B. H. Kim, J. Kim, K. I. Sim, J.-U. Lee, S. Lee, K. Park, S. Yun, T. Kim, A. Nag, A. Walters, M. Garcia-Fernandez, J. Li, L. Chapon, K.-J. Zhou, Y.-W. Son, J. H. Kim, H. Cheong, and J.-G. Park, Coherent many-body exciton in van der Waals antiferromagnet $NiPS_3$, Nature (London) **583**, 785 (2020).

[4] K. Hwangbo, Q. Zhang, Q. Jiang, Y. Wang, J. Fonseca, C. Wang, G. M. Diederich, D. R. Gamelin, D. Xiao, J.-H. Chu, W. Yao, and X. Xu, Highly anisotropic excitons and multiple phonon bound states in a van der Waals antiferromagnetic insulator, Nat. Nanotechnol. **16**, 655 (2021).

[5] X. Wang, J. Cao, Z. Lu, A. Cohen, H. Kitadai, T. Li, Q. Tan, M. Wilson, C. H. Lui, D. Smirnov, S. Sharifzadeh, and X. Ling, Spin-induced linear polarization of photoluminescence in antiferromagnetic van der Waals crystals, Nat. Mater. **20**, 964 (2021).

[6] C.-H. Ho, T.-Y. Hsu, and L. C. Muhimmah, The band-edge excitons observed in few-layer $NiPS_3$, npj 2D Mater. Appl. **5**, 8 (2021).

[7] C. A. Belvin, E. Baldini, I. O. Ozel, D. Mao, H. C. Po, C. J. Allington, S. Son, B. H. Kim, J. Kim, I. Hwang, J. H. Kim, J.-G. Park, T. Senthil, and N. Gedik, Exciton-driven antiferromagnetic metal in a correlated van der Waals insulator, Nat. Commun. **12**, 4837 (2021).

[8] F. Dirnberger, R. Bushati, B. Datta, A. Kumar, A. H. MacDonald, E. Baldini, and V. M. Menon, Spin-correlated exciton–polaritons in a van der Waals magnet, Nat. Nanotechnol. **17**, 1060 (2022).

[9] T. Y. Kim and C.-H. Park, Magnetic anisotropy and magnetic ordering of transition-metal phosphorus trisulfides, Nano Lett. **21**, 10114 (2021).

[10] R. Brec, D. M. Schleich, G. Ouvrard, A. Louisy, and J. Rouxel, Physical properties of lithium intercalation compounds of the layered transition-metal chalcogenophosphites, Inorg. Chem. **18**, 1814 (1979).

[11] M. Piacentini, F. Khumalo, C. Olson, J. Anderegg, and D. Lynch, Optical transitions, XPS, electronic states in $NiPS_3$, Chem. Phys. **65**, 289 (1982).

[12] M. Piacentini, F. Khumalo, G. Leveque, C. Olson, and D. Lynch, X-ray photoemission and optical spectra of $NiPS_3$, $FePS_3$ and $ZnPS_3$, Chem. Phys. **72**, 61 (1982).

[13] M. Piacentini, V. Grasso, S. Santangelo, M. Fanfoni, S. Modesti, and A. Savoia, Study of the valence bands of $FePS_3$ and $NiPS_3$ by resonant-photoemission spectroscopy, Il Nuovo Cimento D **4**, 444 (1984).

[14] M. Kelly, R. Daniels, G. Margaritondo, and F. Levy, Resonant-photoemission identification of the valence states of $NiPS_3$, Solid State Commun. **50**, 233 (1984).

[15] T. Miyazaki, H. Fujimoto, K. Ichimura, K. Lee, S. Hasegawa, and H. Inokuchi, UPS study of $NiPS_3$ and $FePS_3$ crystals using synchrotron radiation, Chem. Phys. **201**, 539 (1995).

[16] A. Kamata, K. Noguchi, K. Suzuki, H. Tezuka, T. Kashiwakura, Y. Ohno, and S.-i. Nakai, Resonant $2p$-$3d$ Photoemission Measurement of MPS_3 (M = Mn, Fe, Ni), J. Phys. Soc. Jpn. **66**, 401 (1997).

[17] M. Yan, Y. Jin, Z. Wu, A. Tsaturyan, A. Makarova, D. Smirnov, E. Voloshina, and Y. Dedkov, Correlations in the electronic structure of van der Waals $NiPS_3$ crystals: An x-ray absorption and resonant photoelectron spectroscopy study, J. Phys. Chem. Lett. **12**, 2400 (2021).

[18] M. Piacentini, V. Grasso, S. Santangelo, M. Fanfoni, S. Modesti, and A. Savoia, Soft x-ray absorption of $FePS_3$ and $NiPS_3$, Solid State Commun. **51**, 467 (1984).

[19] V. Grasso, S. Santangelo, and M. Piacentini, M2, 3 absorption spectra of transition metal ion in $MnPS_3$, $FePS_3$ and $NiPS_3$, Solid State Commun. **60**, 381 (1986).

[20] C. Sugiura, A. Kamata, and S.-i. Nakai, X-ray spectroscopic investigation of the valence-band structure of layered compounds MPS_3 (M = Mn, Fe, Ni, Zn, Mg), J. Phys. Soc. Jpn. **65**, 2152 (1996).

[21] Y. Ohno, Systematic EELS study of layered metal-phosphor-trisulfides MPS_3 (M = Mg, Mn, Fe, Ni, Zn, Cd), Solid State Commun. **67**, 1089 (1988).

[22] M. F. DiScala, D. Staros, A. de la Torre, A. Lopez, D. Wong, C. Schulz, M. Bartkowiak, B. Rubenstein, and K. W. Plumb, Dimensionality dependent electronic structure of the exfoliated van der Waals antiferromagnet $NiPS_3$, arXiv:2302.07910.

[23] F. Roth, A. König, J. Fink, B. Büchner, and M. Knupfer, Electron energy-loss spectroscopy: A versatile tool for the investigations of plasmonic excitations, J. Electron Spectrosc. Relat. Phenom. **195**, 85 (2014).

[24] K. Koepernik and H. Eschrig, Full-potential nonorthogonal local-orbital minimum-basis band-structure scheme, Phys. Rev. B **59**, 1743 (1999).

[25] J. P. Perdew, K. Burke, and M. Ernzerhof, Generalized gradient approximation made simple, Phys. Rev. Lett. **77**, 3865 (1996).

[26] L. Giovanelli, A. Savoyant, M. Abel, F. Maccherozzi, Y. Ksari, M. Koudia, R. Hayn, F. Choueikani, E. Otero, P. Ohresser, J.-M. Themlin, S. S. Dhesi, and S. Clair, Magnetic coupling and single-ion anisotropy in surface-supported Mn-based metal-organic networks, J. Phys. Chem. C **118**, 11738 (2014).

[27] See Supplemental Material at http://link.aps.org/supplemental/10.1103/PhysRevLett.131.256504 for further details on experimental and theoretical methods, additional

photoemission and EELS data, and extended results of DFT and multiplet calculations, which includes Refs. [28–32].

[28] R. O. Kuzian, A. M. Daré, P. Sati, and R. Hayn, Crystal-field theory of Co^{2+} in doped ZnO, Phys. Rev. B **74**, 155201 (2006).

[29] W. Ku, T. Berlijn, and C.-C. Lee, Unfolding first-principles band structures, Phys. Rev. Lett. **104**, 216401 (2010).

[30] E. van Heumen, J. Vuorinen, K. Koepernik, F. Massee, Y. Huang, M. Shi, J. Klei, J. Goedkoop, M. Lindroos, J. van den Brink, and M. S. Golden, Existence, character, and origin of surface-related bands in the high temperature iron pnictide superconductor $BaFe_{2-x}Co_xAs_2$, Phys. Rev. Lett. **106**, 027002 (2011).

[31] L. Landau and E. Lifshitz, *Quantum Mechanics, Non-relativistic Theory*, Course of Theoretical Physics Vol. 3 (Pergamon Press, Oxford, 1958).

[32] F. C. Zhang and T. M. Rice, Effective Hamiltonian for the superconducting Cu oxides, Phys. Rev. B **37**, 3759 (1988).

[33] B. L. Chittari, Y. Park, D. Lee, M. Han, A. H. MacDonald, E. Hwang, and J. Jung, Electronic and magnetic properties of single-layer MPX_3 metal phosphorous trichalcogenides, Phys. Rev. B **94**, 184428 (2016).

[34] J. Yeh and I. Lindau, Atomic subshell photoionization cross sections and asymmetry parameters: $1 \leq z \leq 103$, At. Data Nucl. Data Tables **32**, 1 (1985).

[35] J. van Elp, H. Eskes, P. Kuiper, and G. A. Sawatzky, Electronic structure of Li-doped NiO, Phys. Rev. B **45**, 1612 (1992).

[36] S. Selter, Y. Shemerliuk, M.-I. Sturza, A. U. B. Wolter, B. Büchner, and S. Aswartham, Crystal growth and anisotropic magnetic properties of quasi-two-dimensional $(Fe_{1-x}Ni_x)_2P_2S_6$, Phys. Rev. Mater. **5**, 073401 (2021).

[37] F. S. Khumalo and H. P. Hughes, Reflectance spectra of some $FePS_3$-type layer compounds in the vacuum ultraviolet, Phys. Rev. B **23**, 5375 (1981).

[38] X. Wang, J. Cao, H. Li, Z. Lu, A. Cohen, A. Haldar, H. Kitadai, Q. Tan, K. S. Burch, D. Smirnov, W. Xu, S. Sharifzadeh, L. Liang, and X. Ling, Electronic Raman scattering in the 2D antiferromagnet $NiPS_3$, Sci. Adv. **8**, eabl7707 (2022).

[39] Source code for generating Figs. 1 (d,e) and 4 (theory) together with ancillary numerical data can be accessed through a figshare repository at 10.6084/m9.figshare.24542365.

[40] N. N. Kovaleva, A. V. Boris, C. Bernhard, A. Kulakov, A. Pimenov, A. M. Balbashov, G. Khaliullin, and B. Keimer, Spin-controlled Mott-Hubbard bands in $LaMnO_3$ probed by optical ellipsometry, Phys. Rev. Lett. **93**, 147204 (2004).

[41] A. Koitzsch, E. Müller, M. Knupfer, B. Büchner, D. Nowak, A. Isaeva, T. Doert, M. Grüninger, S. Nishimoto, and J. van den Brink, Low-temperature enhancement of ferromagnetic Kitaev correlations in $\alpha - RuCl_3$, Phys. Rev. Mater. **4**, 094408 (2020).

[42] R. O. Kuzian, O. Janson, A. Savoyant, J. van den Brink, and R. Hayn, *Ab initio* based ligand field approach to determine electronic multiplet properties, Phys. Rev. B **104**, 085154 (2021).

[43] H. Eschrig and K. Koepernik, Tight-binding models for the iron-based superconductors, Phys. Rev. B **80**, 104503 (2009).

[44] C. Monney, V. Bisogni, K.-J. Zhou, R. Kraus, V. N. Strocov, G. Behr, J. c. v. Málek, R. Kuzian, S.-L. Drechsler, S. Johnston, A. Revcolevschi, B. Büchner, H. M. Rønnow, J. van den Brink, J. Geck, and T. Schmitt, Determining the short-range spin correlations in the spin-chain Li_2CuO_2 and $CuGeO_3$ compounds using resonant inelastic x-ray scattering, Phys. Rev. Lett. **110**, 087403 (2013).

[45] J. Kim, M. Daghofer, A. H. Said, T. Gog, J. van den Brink, G. Khaliullin, and B. J. Kim, Excitonic quasiparticles in a spin–orbit Mott insulator, Nat. Commun. **5**, 4453 (2014).

[46] L. J. Sandilands, Y. Tian, A. A. Reijnders, H.-S. Kim, K. W. Plumb, Y.-J. Kim, H.-Y. Kee, and K. S. Burch, Spin-orbit excitations and electronic structure of the putative Kitaev magnet $\alpha - RuCl_3$, Phys. Rev. B **93**, 075144 (2016).

[47] P. Warzanowski, N. Borgwardt, K. Hopfer, J. Attig, T. C. Koethe, P. Becker, V. Tsurkan, A. Loidl, M. Hermanns, P. H. M. van Loosdrecht, and M. Grüninger, Multiple spin-orbit excitons and the electronic structure of $\alpha - RuCl_3$, Phys. Rev. Res. **2**, 042007(R) (2020).

[48] J.-H. Lee, Y. Choi, S.-H. Do, B. H. Kim, M.-J. Seong, and K.-Y. Choi, Multiple spin-orbit excitons in $\alpha - RuCl_3$ from bulk to atomically thin layers, npj Quantum Mater. **6**, 43 (2021).

[49] Q. Zhang, K. Hwangbo, C. Wang, Q. Jiang, J.-H. Chu, H. Wen, D. Xiao, and X. Xu, Observation of giant optical linear dichroism in a zigzag antiferromagnet $FePS_3$, Nano Lett. **21**, 6938 (2021).

[50] M. Yan, Y. Jin, E. Voloshina, and Y. Dedkov, Electronic correlations in $Fe_xNi_yPS_3$ Van der Waals materials: Insights from angle-resolved photoelectron spectroscopy and DFT, J. Phys. Chem. Lett. **14**, 9774 (2023).